Quantitative 3D Tracing of Gene-delivery Viral Vectors in Human Cells and Animal Tissues

Ping-Jie Xiao[1,2], Chengwen Li[1,3], Aaron Neumann[2] and R Jude Samulski[1,4]

[1]Gene Therapy Center, University of North Carolina at Chapel Hill, Chapel Hill, North Carolina, USA; [2]Department of Cell and Developmental Biology, University of North Carolina at Chapel Hill, Chapel Hill, North Carolina, USA; [3]Department of Pediatrics, University of North Carolina at Chapel Hill, Chapel Hill, North Carolina, USA; [4]Department of Pharmacology, University of North Carolina at Chapel Hill, Chapel Hill, North Carolina, USA

Trafficking through a variety of cellular structures and organelles is essential for the interaction between gene-delivery vectors (*i.e.*, adeno-associated virus (AAV) and liposomes) and host cells/tissues. Here, we present a method of computer-assisted quantitative 3D biodistribution microscopy that samples the whole population of fluorescently-labeled vectors and document their trafficking routes. Using AAV as a working model, we first experimentally defined numerical parameters for the singularity of Cy5-labeled particles by combining confocal microscopy and atomic force microscopy (AFM). We then developed a robust approach that integrates single-particle fluorescence imaging with 3D deconvolution and isosurface rendering to quantitate viral distribution and trafficking in human cells as well as animal tissues at the single-particle level. Using this quantitative method, we uncovered an as yet uncharacterized rate-limiting step during viral cell entry, while delineating nuclear accumulation of virions during the first 8 hours postinfection. Further, our studies revealed for the first time that following intramuscular injection, AAV spread progressively across muscle tissues through endomysium between myofibers instead of traversing through target cells. Such 3D resolution and quantitative dissection of vector–host interactions at the subcellular level should significantly improve our ability to resolve trafficking mechanisms of gene-delivery particles and facilitate the development of enhanced viral vectors.

Received 3 July 2011; accepted 18 October 2011; published online 22 November 2011. doi:10.1038/mt.2011.250

INTRODUCTION

Therapeutic gene delivery is becoming one of the major strategies to improve human health. For example, both viral and nonviral vectors (*e.g.*, adenovirus, adeno-associated virus (AAV), liposomes, and nanospheres) have recently been adapted to deliver therapeutic agents in an endeavor to treat human disorders.[1,2] Encapsulation of the intracellularly-acting materials (*i.e.*, nucleotides, proteins) into specialized delivery vehicles (*i.e.*, viral capsids, nanospheres) that can deliver these agents to specific organelle in a controlled fashion is critical to attain efficient and selective pharmacological effects.[3] To achieve such functions, these vectors have to partially or fully transverse a biological maze, which is mainly a multi-step trafficking process from cell surface binding to nuclear entry.[4,5] Consequently, development of therapeutic delivery vectors has concentrated on pharmacological reagents and vector variants that affect these pathways.[6–9] Effective achievement of such efforts requires quantitatively evaluating the biological effect(s) of those reagents or vector variants on these complex trafficking routes and biodistribution of delivery vehicles.

During the past decades, several sophisticated fluorescence microscopy techniques including confocal and total internal reflection fluorescence (TIRF) microscopy have revolutionized our knowledge of specific viral trafficking events in cultured cells.[10,11] For example, confocal microscopy with the assistance of 2D colocalization assay helped to suggest that AAV2 differentially traffic through late and recycling endosomes in a dose-dependent manner,[10] while TIRF microscopy–assisted live cell imaging helped to show that actin disruption drugs could block the retrograde flow of human papillomavirus on cell surface.[11]

However, despite advances of 2D imaging and analysis,[12–14] to date there is no method available to quantify the number and biodistribution of nanoscaled viral particles in animal cells and tissues, which is essential in evaluating the effects of pharmacological reagents and viral vector variants on nanoparticle delivery. For example, many viral vectors have high particle-to-plaque forming unit (pfu) ratios, requiring hundreds to thousands of virions to successfully infect a single cell. This strongly suggests that (i) virions may take several different pathways during infection, (ii) most viral entry and trafficking events might be futile,[4,15] and (iii) a significant number of the particles are defective or not assembled properly.[16] Before one can distinguish productive events from nonproductive ones, it is essential to sample the entire population of intracellular viral particles without bias. Analysis of 2D images, utilized by current microscopy approaches, is not unbiased because it only samples one focal plane of viral particles within infected cells. In addition, each labeled particle is displayed as a discrete and intact multi-voxel fluorescent spot, and the distribution of particles in cells varies on each focal plane along the z-axis. 2D image from any focal plane selected for quantification is arbitrary; therefore, classical pixel-by-pixel colocalization analysis is not suitable to examine intracellular distribution of viral particles that actually exist in 3D. Finally, current centroid-counting

Correspondence: *R Jude Samulski, CB # 7352, Gene Therapy Center, 7113 Thurston Building, The University of North Carolina at Chapel Hill, Chapel Hill, North Carolina 27599-7352, USA. E-mail: rjs@med.unc.edu*

method fails to quantitate viral particles in cells because of the fact that particles may aggregate or move into a subresolutional region like vesicles to give a single fluorescent spot, as is common for nanoparticle trafficking. As a result, no method to date is available for quantitatively determining the biodistribution of nanoscaled vectors in three dimensions (such as outside or inside nucleus, or traversing nuclear membrane).

Here, based on recent advances with computational image processing,[17,18] we developed a sensitive and reliable methodology by integrating single-particle imaging and 3D quantification into classical immunofluorescence to quantitate the trafficking kinetics and biodistribution of nanoparticles in 3D animal cells and tissues. Using Cy5-labeled AAV as a working model, we quantitatively investigated the nuclear entry kinetics and biodistribution of AAV2 in human cells and mouse tissues. This study demonstrates the potential of this methodology in screening pharmacological reagents and vector variants for the development of therapeutic-material delivery strategies as well as in understanding the intracellular behavior of delivery viral vectors *in vitro* and *in vivo*.

RESULTS

Quantitative 3D distribution microscopy

To precisely track and localize labeled particles in cells and tissues, we developed an object-based quantitative 3D distribution microscopy which is composed of two steps: (i) assess the localization of particles and (ii) quantitate the number of particles in each cellular structure. Here, we used localization of particles in nucleus as an example to explain this method. As diagramed in **Figure 1a**-A, five nanoparticles (P1–P5 in four groups G1–G4) are differentially localized in a cell, with P1 inside the nucleus, P2 transversing nuclear membrane, P3–P5 outside of the nucleus, and specially P4 and P5 associated with a subresolutional region (*i.e.*, vesicles with diameter less than 200 nm). Confocal microscope is used to create a z-stack sectioning through the entire cell and generate 3D fluorescence images. Image distortions are a natural aspect of an optical microscope (noise, scatter, glare, and blur) and diminish the contrast and resolution of raw images, thus impairing the accuracy of quantitative image analysis. To counteract these problems, restorative 3D deconvolution is used to reverse the optical distortions, negating the effects of the optical system that are represented by its point spread function (PSF, **Supplementary Figure S1a**). After 3D deconvolution, the fluorescence images are visualized by 3D volume rendering as shown in **Figure 1a**-B, with four fluorescence spots (1–4) formed by corresponding particles.

To determine the localization of each particle in an object-by-object manner, we first employ isosurface rendering by thresholding fluorescence intensity to distinguish signal from the background

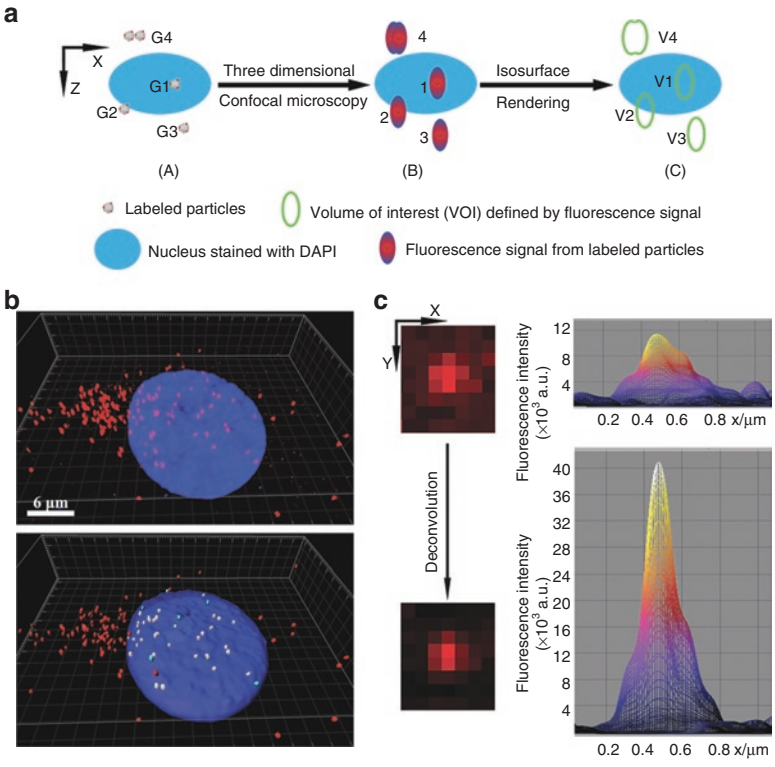

Figure 1 Object-based quantitative 3D distribution microscopy. (**a**) Working model for object-based 3D biodistribution measurement is shown in X/Z dimensions. (A) Actual localization of labeled particles and nucleus, with five particles localized in four optically resolvable groups (G1–G4), (B) expected fluorescence signal (spots 1–4) from four groups of labeled particles by 3D confocal microscopy, and (C) four volume of interest (V1–V4) defined by the fluorescence spots in (B) with the assistance of isosurface rendering. (**b**) Distribution of Cy5-AAV2 particles in HeLa cells at 6 hours postinfection. Upper panel is the fluorescence signal from 3D confocal microscopy, with red Cy5-AAV2 and blue 4′,6′-diamidino-2-phenylindole–stained nucleus. Bar = 6 µm. Lower panel is the isosurface rendering and shows the different localization of viral particles: red is in cytoplasm, cyan is traversing nuclear membrane, and yellow is inside of nucleus. (**c**) Example of 3D deconvolution of fluorescence signal of Cy5-AAV2 particles. This improves the signal-to-noise ratio and dimensional resolution of fluorescence signal from a single Cy5-AAV2. 3D surface plots (right panel) of the fluorescence signal from a single particle before and after deconvolution were generated by ImageJ. Pixel size in X and Y is 0.13 × 0.13 µm. AAV, adeno-associated virus.

(**Supplementary Figure S1a**, dashed blue line). With this method, we create a volume of interest (VOI) for each fluorescence spot from an optically resolvable particle group (**Figure 1a**-A: G1–G4; and **Supplementary Video S1**: isosurface rendering). The localization of each particle is then determined by the amount of 4′,6′- diamidino-2-phenylindole (DAPI) signal within its VOI (**Figure 1a**-C: V1–V4). Specifically, the mean fluorescence intensity (MFI) of DAPI in V1 is the same as that in nucleus, demonstrating that P1 is inside the nucleus; the MFI of DAPI in V3 and V4 is the same as that in the cytoplasm, but much lower than that in nucleus, demonstrating that P3–P5 are outside the nucleus; and the MFI of DAPI in V2 is between those in nucleus and in cytoplasm, demonstrating that P2 is traversing the nuclear membrane.

To count the number of particles, classical centroid-counting method fails when several particles associate with a subresolutional region and display as a single fluorescent spot (**Figure 1a**-B: spot #4), which is very common in nanoparticle trafficking. In addition, the amount of dyes (or dye-labeled particles) should be calculated by the number of emitted photon or fluorescence intensity instead of fluorescence volume,[12,19] as there is no linear correlation between the amount of dyes and fluorescence volume (**Supplementary Figure S2**).[20] To quantitate particles including those within subresolutional regions, we calculate such number using the total fluorescence intensity (TFI) of each fluorescence spot by the following formula: number of particles in structure-X = $\sum TFI_{strX}/mTFI_s$, in which TFI_{strX} denotes the TFI of fluorescence spots formed by labeled particles in cellular structure X and $mTFI_s$ denotes the mean value of TFI experimentally calculated from fluorescence spots formed by a single particle. Using quantitatively-labeled fluorescence beads (InSpect Image Intensity Calibration beads from Invitrogen), we demonstrated that TFI but not volume linearly correlated with the amount of dyes on beads (**Supplementary Figure S2a**) and the number of dye-labeled objects can be precisely calculated from TFI (**Supplementary Figure S2b**), which validated the accuracy of this intensity-based quantification. In addition, compared with earlier studies,[12,19] this object-by-object quantification method only calculates the signal from viral particles but not the automatically system-generated noise signal prevalent in the digital images because these noise are usually bright fluorescence spots with only one or two pixels/voxels that are filtered away from the particle-formed fluorescence spots with 10 or more voxels (**Figures 1b,2c,3a**). Such feature further improves the precision of this method.

AAV particle labeling, localization, and quantification

With this method, one is able to quantitate the biodistribution of nanoscaled particles in cells/tissues by specifying the number and localization of particles in each cellular structure. In the following context, we quantitate the distribution of Cy5-AAV2 particles in HeLa cells at 6 hours postinfection (p.i.) to fully demonstrate this method.

Labeling viruses with fluorochromes has been extensively used in imaging particle trafficking.[11] We chemically conjugated the effect of viral particles with Cy5 to minimize autofluorescence in cells and tissues. Electron microscopy data demonstrated that the physical morphology of AAV2 was not affected by Cy5 conjugation and most of the labeled virions remained as single particles (**Supplementary Figure S3a**). Labeling did not impact transduction efficiency significantly as indicated by green fluorescence protein (GFP) reporter gene assay (**Supplementary Figure S3b,c**). SDS-PAGE and fluorography of Cy5-AAV2 demonstrated that fluorochromes were specifically coupled to all three capsid proteins (VP1,2,3) as indicated by three fluorescence bands (**Supplementary Figure S3d**). This specificity of labeling was validated in human cells using mouse monoclonal antibody A20 which only recognizes the intact AAV2 particles (**Supplementary Figure S3e**). These results demonstrated that both morphology and functionality (A20 binding and infectivity) of these labeled virions are the same as unlabeled ones.

At 6 hours p.i. with Cy5-AAV2 at 5,000 vector genomes per cell (vg/cell), HeLa cells were fixed and their nuclei were stained with DAPI. A Zeiss710 confocal fluorescence microscope was used to create a *z*-stack sectioning through the entire cell for each fluorochrome at the optimal *z*-step (well-characterized Nyquist sampling frequency). We employed AutoDeblur software (Media Cybernetics) for the deconvolution using an iterative constrained blind algorithm to remove out-of-focus haze, blur, and noise. After 3D deconvolution, the fluorescence signal from AAV particles was visualized by 3D volume rendering (**Figure 1b**). Consistent with theoretical confocal PSF,[20] the fluorescence signal from a labeled particle is shaped as prolate-spheroid in 3D, with an approximate equatorial radius $a = 0.2–0.3\,\mu m$ and polar radius $b = 0.3–0.4\,\mu m$, which resulted in the volume range of less than $0.13\,\mu m^3$. These signals with prolate-spheroid-shape had improved signal-to-noise ratio up to three- to fourfold (**Figure 1c**). Resolution was also enhanced in all three dimensions evaluated by full width at half maximum (0.15–0.2 μm in X/Y and 0.3 μm in Z compared with standard confocal resolution limit of 0.3–0.4 μm in X/Y and 0.6 μm in Z, **Figure 1c**, **Supplementary Figure S1**). We then employed isosurface rendering module in IMARIS software (Bitplane, Zurich, Switzerland) to generate VOIs for the signals from each optically resolvable Cy5-AAV2 group and thereafter determined the localization of Cy5-AAV2 particles to nucleus by DAPI signal. As shown in lower panel of **Figure 1b**, red spots represent the particles outside of nucleus, cyan spots represent the particles associated with nuclear membrane, and yellow spots represent the particles inside of nucleus. $\sum TFI_{strX}$ was then calculated by the TFI_{strX} for each fluorescence spot. To quantitate the particles in each type of localization, we derived the value of $mTFI_s$ in the following studies.

We characterized the fluorescent signal of a single Cy5-AAV2 particle by three parameters (volume, MFI, and TFI). $4–6 \times 10^7$ Cy5-AAV2 particles were loaded onto grid coverslips to yield a distribution of ~1 particle per $5\,\mu m^2$. Uniformly labeled particles were obtained as indicated by confocal microscopy of Cy5-AAV2 on the coverslip (**Figure 2a**, left). Profiles of fluorescence signal intensity for two representative Cy5-AAV2 particles follow Gaussian distribution (**Figure 2a**, right), suggesting that fluorescence signal was from single particles.[11] The fluorescence signal (thresholded as dashed blue line in **Supplementary Figure S1a**) from Cy5-AAV2 had a diameter of 0.5–0.6 μm, comparable to the fluorescence signal generated by other nanoscaled viruses (*e.g.*, SV40).[11] 3–5 regions from each coverslip were imaged using the microscope settings for quantitative analysis (see Materials and Methods), and

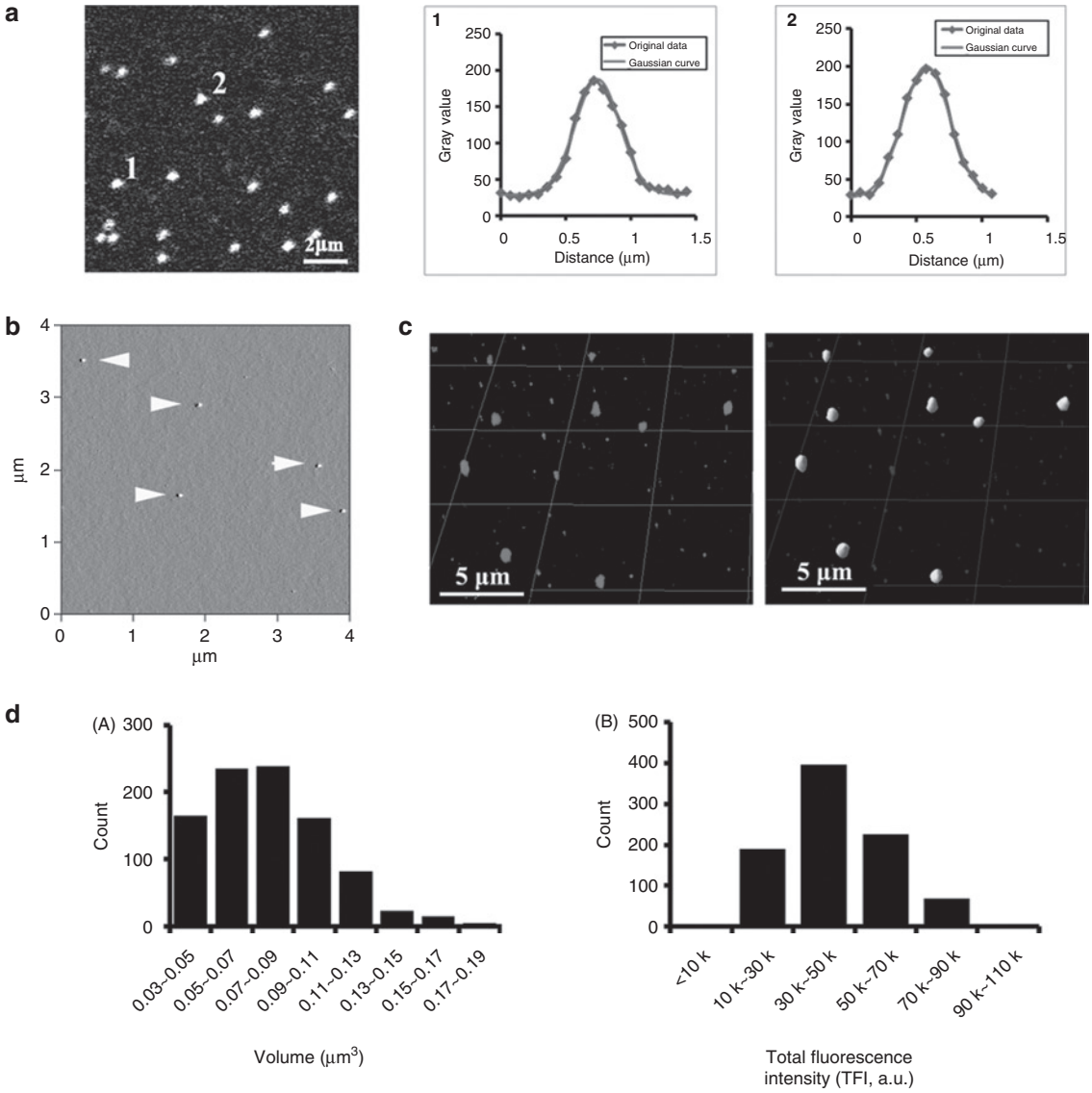

Figure 2 Characterization of fluorescence signal for single Cy5-AAV2 particles. (**a**) Representative confocal image (left) of Cy5-AAV2 bound to coverslip. Bar = 2 μm. Representative fluorescence intensity profiles (right 1–2) of two Cy5-AAV2 particles (indicated at left). (**b**) Atomic force microscopy image of Cy5-AAV2 particles (arrowheads) from the same glass coverslip as in **a** demonstrated the dispersity of viral particles on the coverslip. (**c**) 3D reconstruction of deconvolved confocal images (left: Cy5-AAV2 in red) and subsequent 3D isosurface rendering images (right: Cy5-AAV2 in yellow). Bar = 5 μm. (**d**) Histograms of volume (A) and total fluorescence intensity (B) for all Cy5-AAV2 particles recorded from the coverslip in **a** and **b**. The mean values of total fluorescence intensity was 44834 ± 16447.3 a.u. AAV, adeno-associated virus.

2–3 *Z*-stack images were taken for each region. The distribution of Cy5-AAV2 on the same regions was verified using atomic force microscopy. Only the regions on which the minimum distance between every two physically dissociated Cy5-AAV2 particles was larger than 0.5 μm (**Figure 2b**) were chosen for later quantification. Thus, we demonstrated that each fluorescence spot visualized by fluorescence microscopy represented a single Cy5-AAV2 particle. Images from these chosen regions were processed with 3D deconvolution, reconstruction, and isosurface rendering (**Figure 2c**). Three statistics (volume, Cy5 MFI, and Cy5 TFI) of each isosurface-coated fluorescence spot were used to define the singularity of labeled particles. Volume was plotted for all fluorescent objects (**Figure 2d**-A) and could fit to a Gaussian curve indicating a normal distribution. According to theoretical confocal PSF,[20] we defined Cy5-AAV2 objects with volume smaller than 0.13 μm^3 as the 3D fluorescence pattern for a single Cy5-AAV2. These defined single Cy5-AAV2 objects had a mean value of Cy5 TFIs at 44834 ± 16447.3 arbitrary units (a.u.) (**Figure 2d**-B) and a mean value of Cy5 MFI at 2438 ± 310.6 a.u. (**Supplementary Figure S5a**).

The complexity of the cellular environment may affect the fluorescent properties from a single Cy5-AAV2. We analyzed whether single Cy5-AAV2 particles on glass had similar fluorescent properties on cells. Briefly, we incubated 5,000 Cy5-AAV2 per HeLa cells (over a surface area of ~2,000 μm^2) at 4 °C for 40 minutes to allow a dispersed distribution of Cy5-AAV2 particles over the cell surface (**Figure 3a**). Specificity of viral fluorescence signal was verified by comparison to nonlabeled AAV2 infected

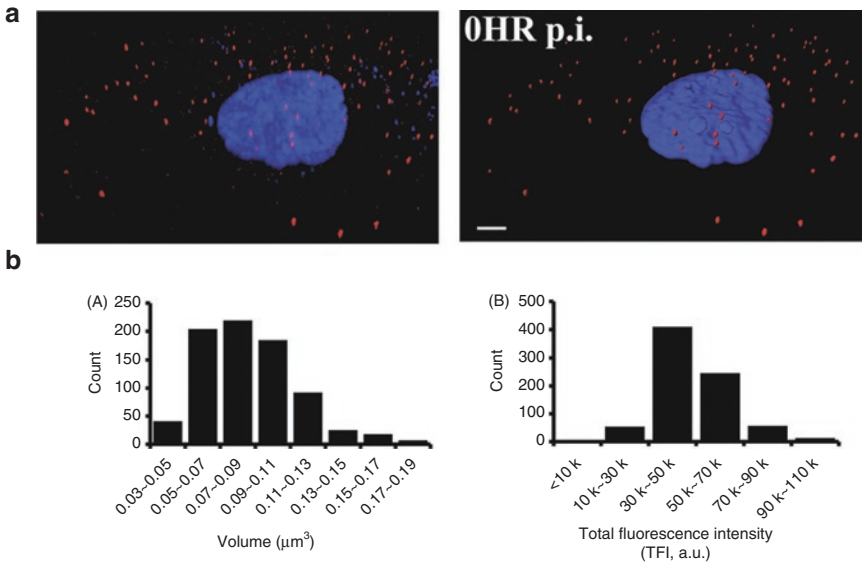

Figure 3 Fluorescence properties of single Cy5-AAV2 particles within cells. HeLa cells were incubated with Cy5-AAV2 (5,000 vg/cell) and fixed and nuclei were stained with 4′,6′-diamidino-2-phenylindole. Stacks of images throughout the cells were taken using a Zeiss710 confocal microscope. (**a**) Representative 3D confocal image of Cy5-AAV2 within cells after being deconvolved and reconstructed (left). Right panel shows the corresponding 3D isosurface rendered image. Bar = 5 μm. (**b**) Histograms of volume (A) and total fluorescence intensity (B) for all Cy5-AAV2 particles within cells (n = 5) as calculated by Imaris program. The mean value of total fluorescence intensity was 47,568 ± 13,345.5 a.u. AAV, adeno-associated virus.

cells (**Supplementary Figure S4**). We then collected the imaging data and analyzed the three parameters (volume, MFI, and TFI) exactly as described above for *in vitro* characterization. The distribution of volumes was almost identical to the results from the analysis on coverslip (**Figures 2d**-A,**3b**-A). The same range of volumes (≤0.13 μm^3) was used to define the fluorescence signal from single Cy5-AAV2 in cells. In the cellular environment, single Cy5-AAV2 objects have a mean value of Cy5 TFIs at 47568 ± 13345.5 a.u. (**Figure 3b**-B) and Cy5 MFI at 2516 ± 256.5 a.u. (**Supplementary Figure S5b**), which is not significantly different from the values determined on coverslip. Consistency between the fluorescent signal from coverslip and cell culture supports that our characterization and quantification by this method is reliable. With these calculated mTFIs (=47568 a.u.), we then determined the number of Cy5-AAV for each location at 6 hours p.i.: 150 in the whole cell, 37 in nucleus, 6 associated with nuclear membrane, and 107 localized in cytoplasm (**Figure 1b**, **Supplementary Video S2**).

With this scenario, the subset of Cy5-AAV2 fluorescence spots with specific nuclear localization can be quantitated by DAPI fluorescence signal within each viral VOI and calculated mTFIs (**Supplementary Video S2**). By applying isosurface rendering to the nuclear DAPI signal, the relative localization between AAV2 particles and nucleus can be easily and unambiguously visualized (**Supplementary Video S2**). Compared with previous studies,[12,13,19] this method not only allows one to assess the viral distribution from the view of entire population but also allows one to locate each individual particle into finer subcellular structures (*i.e.*, inside/outside nucleus or traversing nucleus, as shown in **Figure 1b**). By determining the fluorescence parameters for single particles, this method, for the first time, also allows one to quantitate the number of virions in various cellular structures. For example, including nuclear targeting, colocalization of AAV2 with other specific cellular structures (*e.g.*, AAV-cell membrane, AAV-lysosome) and corresponding trafficking kinetics were quantitatively investigated using this method.

Kinetics of AAV2 trafficking in endo/lyso vesicles and nucleus

Intracellular trafficking in small vesicles like endosomes and lysosomes is essential for productive viral infection. For example, AAV2 has been shown to undergo successive endosomal trafficking and sorting after viral entry.[10] We tested the applicability of this method toward elucidating these essential events using lysosomal association of AAV2 as an example. HeLa cells were incubated with Cy5-AAV2 (5,000 vg/cell) at 4 °C for 40 minutes. After removing unbound virions, cells were incubated at 37 °C and harvested at 0 hour, 2 hours, 4 hours, 8 hours, and 13 hours p.i. and fixed with paraformaldehyde. Lysosomes were labeled with monoclonal Lamp1 antibody. *Z*-stack images were captured through the entire cell using a Zeiss LSM710 laser scanning confocal microscope. After 3D deconvolution and reconstruction of image stacks, we measured the association between lysosomes and AAV2 particles over time. Our results demonstrated that about 40% of intracellular AAV2 consistently associated with lysosomes between 2 hours and 13 hours after infection (**Supplementary Figure S6**).

Nuclear entry of either viral proteins or genetic material, following the small vesicle trafficking, is one of the rate-limiting steps in most viral infection. Extensive effort has been made to block this step in antivirus strategies or to improve the efficiency of this step for more efficient gene delivery.[15,21–23] Like several DNA viruses,[23] AAV2 has to enter the cell nucleus to complete its life cycle.[15,24] However, such trafficking kinetics as well as the mechanism through which AAV enters nucleus remains unknown due to the lack of a quantitative method to study this process. Here, we demonstrated the use of

3D tracking of single viral particles to explore the dynamics of AAV2 nuclear entry in cultured cells.

Experiments were carried out as lysosomal association studies, and nuclei were stained with DAPI. After 3D deconvolution and reconstruction of image stacks, we quantitatively documented the kinetics of AAV2 nuclear targeting (**Figure 4**, **Supplementary Video S3–S5**). We observed that the number of viral particles (~200) associated with the cell did not change significantly over the time period we observed (**Figure 4b**-A). On average, 0% and 14% of total intracellular viral particles were found in the nucleus at 0 hour and 2 hours p.i., respectively, and this percentage increased to 22% at 4 hours, 28% at 8 hours, and 27% at 13 hours (**Figure 4b**-B). With the previous measured mean value of Cy5 TFI (47568 a.u.) for a single Cy5-AAV2, the corresponding viral particle numbers in the nucleus were 27, 38, 48, and 41 at 2 hours, 4 hours, 8 hours, and 13 hours, respectively (data not shown). These results suggest the following dynamics of AAV2 nuclear targeting: (i) Half of the nuclear targeting events happened within the first 2 hours p.i., with the remainder occurring between 2 and 8 hours p.i. This correlates well with the fact that reporter gene (GFP) expression can be detected as early as 6–8 hours p.i. (ii) The relative number of AAV2 in the nucleus appears to level off at 8 hours p.i., with about 30% (48 out of 170) intracellular AAV2 particles on average located in the nucleus. This result is consistent with an earlier report which found that a similar percentage of AAV genome (~30%) ended up in the nucleus.[25] These results were summarized into an *in vitro* model (**Figure 6a**) and quantitatively documented in a table (**Figure 6c**, upper panel). Remarkably, the percentage of AAV2 associated with the nuclear membrane (~12%) at 2 hours p.i. did not change when the viral dosage was increased to 25,000 v/cell. However, nuclear entry efficiency at 2 hours p.i. with 25,000 vg/cell (~4%) was significantly decreased (threefold) compared to that with 5,000 vg/cell (~14%) (**Figure 4c,d**). These results suggest that limited sites for viral entry are available on the nuclear membrane or limited trafficking routes are available for AAV2 to enter nucleus. Accordingly, the

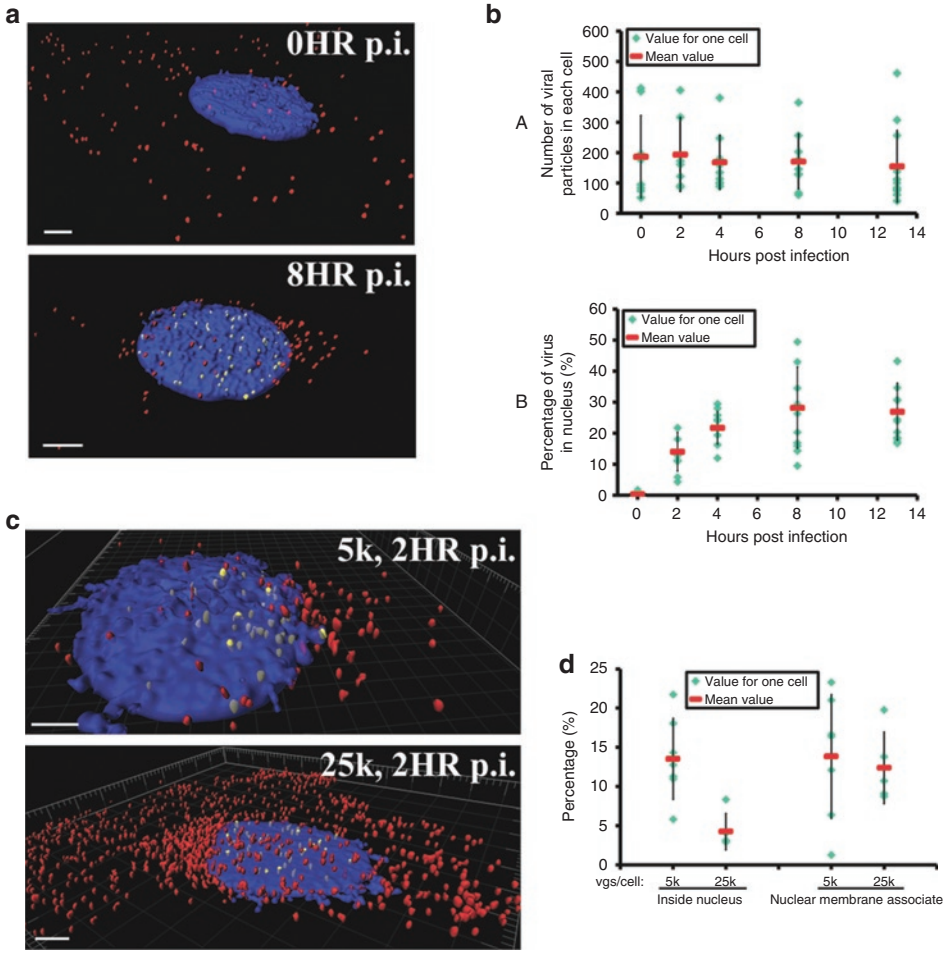

Figure 4 Kinetics of Cy5-AAV2 nuclear targeting. HeLa cells were incubated with Cy5-AAV2 (**a,b**: 5,000 vg/cell; **c,d**: 5,000 or 25,000 vg/cell) at 4 °C for 40 minutes and then transferred to 37 °C incubator. Cells were then fixed at 0, 2, 4, 8, and 13 hours and nuclei were stained with 4′,6′-diamidino-2-phenylindole. The number of viral particles within cells was calculated using the mean value of Cy5 total fluorescence intensity (47568 a.u.) determined in Figure 3b-B. (**a**) Representative 3D isosurface images of Cy5-AAV2 within cells at 0 hour and 8 hours postinfection. Viral particles in nuclei are highlighted as yellow. Bar = 5 µm. (**b**) Plots of total number of viral particles (A) and percentage of intranuclear viral particles (B) in each cell. (**c**) Representative 3D isosurface images of cells infected at 5,000 or 25,000 vg/cell at 2 hours postinfection. Viral particles in nuclei are highlighted as yellow. Bar = 5 µm. (**d**) Percentage of intranuclear and nuclear membrane–associated viral particles as shown in **c**. Cyan diamond represents data from individual cells (n = 10–20), red bars represent mean value of each time point, and error bars represent SD. AAV, adeno-associated virus.

transduction efficiency measured by transgene GFPsc expression at 25,000 vg/cell is only about threefold of that at 5,000 vg/cell (**Supplementary Figure S7**).

Trafficking kinetics in mouse muscle

The ultimate goal of studying particle trafficking is to elucidate the behavior of viral and nonviral vectors in tissues and animals. The *in vivo* setting provides the most applicable information for the development of efficient gene-delivery vectors. Current method of studying the distribution of viral vectors *in vivo* using reporter gene assays tracks only the virions that successfully transduce cells. Given that the vast majority of virions are likely to be futile in infection, reporter gene imaging provides a biased understanding of virion distribution that can easily lead to misinterpretation of the pharmacology of these agents, resulting in failed development of antiviral and therapeutical delivery vectors.[4,26] To circumvent this problem, we have successfully tracked all AAV particles, both infectious and abortive, in mouse muscle over time.

After local injection with Cy5-AAV2 particles, mouse hind limb muscle were collected at 0.5, 2, 4 hours and 6 days. Reporter gene (GFP) expression spread up to several muscle fibers away from the injection site, indicated by Indian ink (arrows in **Figure 5a,b**), and was stronger in those fibers closer to the injection site than in the fibers distal from injection site at 6 days p.i. (**Figure 5a**). The immediate question is whether this distribution pattern represents the spreading of GFP molecules or viral particles across the muscle fibers. Our results showed that, in contrast to Indian ink remaining local to the site of injection (**Figure 5b**, upper panel), AAV particles migrated from the injection site into the neighboring fibers (three muscle fibers away from the injection site). We observed that numbers of AAV particles in the surrounding fibers and in nuclei increased from 0.5 hour to 4 hours (**Figure 5b**, lower panel and **Supplementary Video S6,S7**). Almost all Cy5-AAV2 particles were located at the site of injection after 0.5-hour p.i. A few viral particles were observed on the side of fibers (sarcoplasm) adjacent to the injection site at 2 hours p.i. A large amount of viral

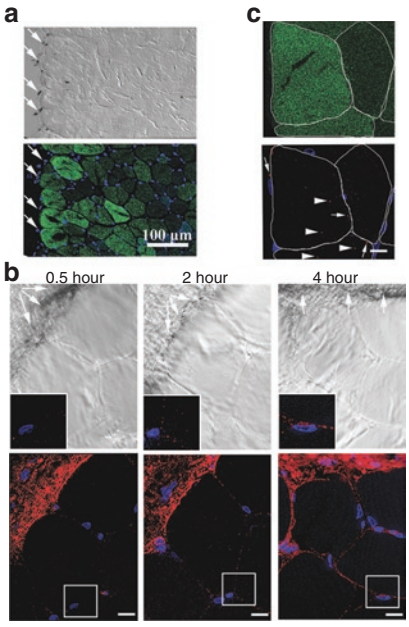

Figure 5 Trafficking of AAV2 in mouse muscle. (**a**) Site of AAV injection is visualized by Indian ink (black spots in upper panel) and is indicated by arrows and corresponding reporter gene GFP expression (green) in muscle at 6 days postinjection (lower panel). Bar = 100 µm. (**b**) Distribution of Cy5-AAV2 particles in mouse muscle at 0.5, 2, and 4 hours postinjection. Upper panel shows the differential interference contrast (DIC) images with the injection site indicated by arrows. Lower panel shows the localization of Cy5-AAV2 particles (red) and nuclei (blue). The inserts in upper panel are the magnified view of selected regions in lower panel (white boxes). Bar = 10 µm. (**c**) Cy5-AAV2 particles were detected inside the muscle fibers at 6 days postinjection. Upper panel shows the expression of reporter gene GFP in muscle fibers. Lower panel shows the Cy5-AAV2 particles (red) and nuclei (blue). Individual muscle fibers are outlined by curved white lines. Arrowheads indicate the viral particles inside the fibers and arrows indicate the viral particles along the side of muscle fibers. Bar = 10 µm.

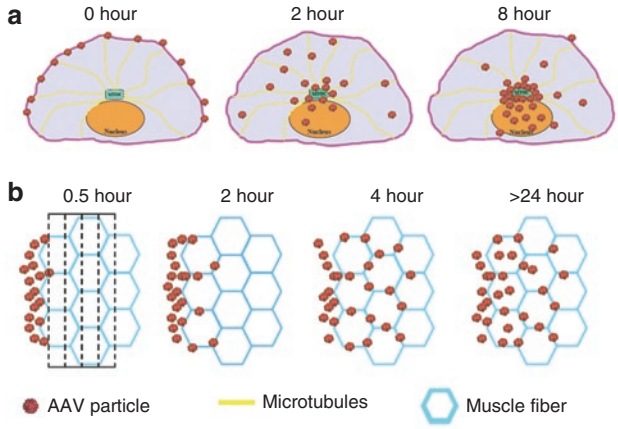

c

In vitro (MOI = 5,000 vgs/cell)

	Total number of AAV	AAV traversing nuclear membrane		AAV in nucleus	
	Mean number/per cell	Mean number per cell	Mean percentage (%)	Mean number per cell	Mean percentage (%)
0 hour	186	0	0	0	0
2 hour	193	29	15	27	14
4 hour	168	21	12	28	22
8 hour	170	24	14	48	28
13 hour	152	23	14	41	27

In vivo (2E+09 vgs/injection)

	Total number of AAV within the region		Number of AAV traversing nuclear membrane per nucleus		No. of AAV in nucleus per nucleus		
Hours p.i.	2 hours	4 hours	2 hours	4 hours	2 hours	4 hours	6 days
Region I	758	3252	14	27	13	148	Not detectable in most nuclei
Region II	597	2518	4	27	6	23	
Region III	54	1186	0	12	0	10	
Region IV	N.A.	699	N.A.	1	N.A.	4	

Figure 6 Schematic and quantitative documentation of AAV2 trafficking in vitro and in vivo. (**a**) Model for AAV2 infection in cell culture. After binding to the cell surface at 0 hour, AAV2 particles are transported via microtubules toward the perinuclear region (typically microtubule organization center, MTOC) within the first 8 hours after viral inoculation. Progressive nuclear entry is observed during the first 8 hours postinfection, with about 30% of viral particles in the nucleus at 8 hours postinfection. (**b**) Model for AAV2 trafficking mouse muscle shown in cross-sectioned view. AAV2 particles traffic from the injection site to distal myofibers through the endomysium between those fibers. Some AAV particles penetrate the muscle fibers, but only at later time point (≥24 hours). To quantitatively document the intramuscular trafficking in **c** (**Table 2**), four regions (I–IV) were defined from the injection site to distal myofibers, and the width of each region is about half of myofiber's diameter. (**c**) Quantitative documentation of AAV2 distribution and trafficking kinetics in cultured HeLa cells (**Table 1**) and mouse muscles (**Table 2**). AAV, adeno-associated virus.

particles appeared on the side of fibers close to (three muscle fibers away from) the injection site at 4 hours p.i. Such trafficking kinetics was summarized in an *in vivo* trafficking model (**Figure 6b**) and quantitatively documented in a table (**Figure 6c**, lower panel). During this time period, viral particles were only observed along the side of muscle fibers (sarcoplasm) but not inside the fibers prior to 4 hours p.i. (**Figure 5b**, lower panel) and the number of AAV capsids in nucleus was increased over time (**Figure 6c**). This observation suggests that viral particles after intramuscular injection are likely to spread through the endomysium between muscle fibers, rather than by transcytosis. In addition, at 6 days p.i., AAV capsids were only observed along and inside the muscle fibers but not detectable in most of the nuclei (**Figures 5c,6c**). This observation suggested that most AAV genome should be readily released quite rapidly *in vivo*.

DISCUSSION

Understanding how nanoparticles travel through the cellular structures and how pharmacological reagents can affect viral trafficking is essential for the development of enhanced gene therapy vectors (*e.g.*, polymers, adenovirus, and AAV).[3] Fluorophore labeling of particles has been mainstay in studying the dynamics of particle trafficking.[10,11] While a fancy research tool, current molecular tracking and 2D imaging analyses have significant limitations in studying classical viral trafficking and biodistribution,[13,14] in which temporal resolution is not the primary interest. For example, sampling all intracellular viral particles and quantitatively studying their distribution and trafficking kinetics in 3D animal cells and tissues has not yet been achieved. Although investigation of biodistribution and trafficking kinetics of DNA carrier vectors have been attempted previously,[12,13] these studies are 2D imaging analyses that have limitations in quantitatively characterizing the viral behavior in 3D cellular structures. For example, classical 2D imaging and analysis can lead to arbitrary results, as the distribution patterns in different focal planes vary along the *z*-axis of confocal images. As a result, neither distribution data gained from a specific focal plane nor that simply summed up from all focal planes is able to correctly reflect the behavior of virus in cells. Recently, Chen *et al.* studied the trafficking kinetics of plasmid carriers by measuring the volume of fluorescence spot generated by labeled particles.[19] As known, the amount of dye molecules (or dye-labeled particles) in a subresolutional region (diameter < 150 nm) should be calculated by the amount of emitted photons linearly reflected by fluorescence intensity in confocal images[20,27] but not by fluorescence volume, as there is no linear correlation between number of dye molecules (or labeled particles) and fluorescence volume (**Supplementary Figure S2a**). As a result, the amount of emitted photons or fluorescence intensity instead of fluorescence volume should be used to quantitate dye-labeled subresolutional-sized particles (**Supplementary Figure S2**). The method described in this study directly uses fluorescence intensity information to quantitatively determine the number and distribution of nanoscaled particles in three dimensions (**Supplementary Figure S2**, **Figures 2d**-B,**3b**-B), which is fundamentally different from the volume-based method.[19] In addition, restorative 3D deconvolution was also applied to appropriately counteract the image distortions caused by optical systems to increase the accuracy of this 3D image analysis (**Supplementary Figure S1**).[20] In brief, this method has employed multiple strategies including isosurface-assisted object-by-object analysis (**Figure 1b**), intensity-based calculation (**Supplementary Figure S2**), and restorative 3D deconvolution (**Supplementary Figure S1**) to significantly improve the accuracy of 3D image quantification. Compared with previous studies, including the improved precision of image quantification, this method not only allows one to view the particle trafficking from an entire viral population (**Figures 4,6c**) but also, for the first time, allows one to locate each individual particle into finer subcellular structures (*i.e.*, inside/outside nucleus or traversing nucleus, as shown in **Figure 1b** and detailed localization in muscle as shown in **Figure 5c**). By determining the fluorescence parameter for a single Cy5-AAV2 virion (**Figures 2,3**), this method also allows one to quantitate the absolute number of particles in each cellular structure such as nucleus (**Figure 4**), microtubules, and cell surface (data not shown) as well as subresolutional vesicle structures like endo/lysosomes (**Supplementary Figure S6**), which have never been reported previously. Finally and importantly, this method, for the first time, allows one to quantitatively investigate particle biodistribution/trafficking in animal tissues (**Figure 5**), which have not been documented by any of the above method.

Our electron microscopy data demonstrates that almost all Cy5-AAV2 virions we used in this study are full particles (**Supplementary Figure S3a**). The labeled virions are shown to preserve the capsid integrity as determined by A20 antibody binding (**Supplementary Figure S3e**) and have similar infectivity as nonlabeled AAV2 (**Supplementary Figure S3b,c**). These labeled virions are also shown to have the normal ability to bind heparan sulfate and migrate on microtubules (data not shown). Using these Cy5-AAV2 that preserve the same morphology and functionality as unlabeled ones, we have generated a body of interesting and biologically meaningful results consistent with previous reports as well as several novel observations that have never been documented previously. For example, we have quantitatively demonstrated that the majority of AAV2 are bound to the cell surface as single particles even at a high multiplicity of infection and the binding of AAV2 can be blocked by incubating the virus with heparin or incubating cells with heparanase (data not shown), supporting previous reports showing heparan sulfate is the primary receptor for AAV2.[5,28] We then demonstrated that AAV2 can migrate on microtubules and that disruption of the microtubule network impaired the nuclear targeting of AAV2 (data not shown). The kinetics of AAV2 trafficking in small vesicles like lysosomes was illustrated using this quantitative microscopy method (**Supplementary Figure S6**). In addition, we also explored the kinetics of AAV2 nuclear trafficking, one of the most important events in AAV infection, by quantitating the number and percentage of AAV particles in nuclei over time (**Figures 1b,4,6c**). Importantly, we have, for the first time, quantitatively characterized the trafficking behavior of AAV2 in mouse muscle tissue (**Figures 5b,6c**), providing rationale for the pattern of viral transgene expression *in vivo*. We will discuss some of these findings in detail in the following text.

Nuclear entry is regarded as the most critical and rate-limiting step for the life cycle of most DNA viruses (*e.g.*, adenovirus,

herpesvirus, and parvovirus).[23,29] Blocking the nuclear entry is an alternative way to block viral replication,[21,23] and on the other hand, facilitating the nuclear entry of viruses has been a promising strategy to improve viral vectors for gene delivery.[15,22,30,31] Several groups have suggested that AAV entered nucleus as intact virions.[5,15,24] For example, the Kleinschmidt group demonstrated that intact AAV2 particles enter the nucleus, as nuclear injection of the A20 antibody can block AAV2 infection and disassembled AAV particles are not detected by B1 antibody until 20 hours after infection.[24] Our group showed that AAV enters the nucleus as intact virions and nuclear virions could be extracted and used to reinfect new cells.[15] These most recent studies suggest that AAV enters nucleus as intact virions and then uncoats there. However, the kinetics of AAV nuclear targeting has not been precisely documented and the exact route/site for viral nuclear entry is highly controversial. The method described herein was used to quantitatively investigate the viral nuclear entry step. Our microscopy analysis of AAV documented the kinetics of nuclear entry over 13 hours p.i. (**Figures 4,6c**), summarized in the *in vitro* model (**Figure 6a**). The result showing that about 30% of bound AAV2 particles entered nucleus, together with the observation showing that only about 4%–5% (~200 out of 5,000 virions/cell) of particles in the medium attached to cell surface, suggests that only 1%–2% of AAV2 virions will eventually enter the nucleus and express. Such binding efficiency was verified by quantitative polymerized chain reaction (data not shown) and also reported by other studies for other AAV serotypes.[32] This low binding efficiency is due to the nature of biochemical reaction between ligands (AAV2) and receptors (heparan sulfate on cell surface) rather than the quality of AAV prep because the unbound particles remaining in the medium can be transferred to successfully infect new cells as well. These results propose the existence of a noninfectious trafficking pathway as another reason for the high particle-to-pfu phenomena in AAV infection in addition to the defective particles in AAV preparations. We also noticed a wide variation in the number of nuclear particles per cell at every time point (**Figure 4b**). This supports a highly heterogeneous susceptibility of each cell to AAV2 infection and explains the variation of AAV2 transgene GFP expression among individual cells (unpublished data). As a result, by quantitating the number of virions in a single cell as accessible by this method, one will be able to correlate the number of viral particles in a cell with the amount of transgene expression to address questions like how many virions are needed to express a certain amount of transgene. Typically, one will be able to observe the expression of double-stranded GFP transgene *in vitro* at about 6–8 hours after infection. Given the several hours required for the maturation of a GFP molecule to give fluorescence,[33] such observation indicates that viral particle should enter nucleus and release genome within couple of hours p.i. The kinetics of AAV nuclear trafficking revealed in this study clearly demonstrated the early AAV2 nuclear entry events within 2 hours p.i. (**Figure 4b**), which provides a molecular rational for such a gene expression profile. In dose response studies, the number of virions in the nucleus does not increase linearly with the number of nuclear membrane–associated virions at 2 hours p.i. (**Figure 4d**). This result suggests that there may be limited sites/routes for AAV2 nuclear entry through the nuclear membrane and provides a sound explanation for the observation that the fold increase in virion dosage does not translate to equivalent fold increase in transduction (**Supplementary Figure S7**). Experiments to confirm this hypothesis are ongoing. With such scenario, this method enables one to quantitate the effects of pharmacological drugs and AAV variants on the nuclear transportation of AAV particles to facilitate the direction towards improving this vector's performance.

Similar to the documentation of nuclear entry dynamics, the kinetics of viral trafficking through other cellular structures (*i.e.*, small vesicles, cell surface, microtubules) can also be documented with this method (**Supplementary Figure S4**, and data not shown). The spatial-temporal distribution of all viral particles within the host cells throughout the entire trafficking pathway can be determined by integrating all the information regarding the kinetics of virions in various cellular structures. It is noted that about 1:100 rAAV2 particles are infectious consistent with a recent report,[16] suggesting that only 1 out of 100 viral particles in culture medium will successfully infect a cell in the culture dish. Our study shows that only about 5% of rAAV2 in the medium will attach to the cell surface for internalization (as suggested by **Figure 4b**). Our heparin competition and heparanase treatment studies demonstrate that all particles tracked in these experiments were 100% positive for first step in infectious pathway (*i.e.*, viral binding), making the above observations relevant irrespective of the particle-to-infectious-unit ratio (data not shown).

Understanding the distribution of viral and nonviral vectors *in vivo* is extremely valuable to advance current drug/DNA delivery strategies. In this study, we have successfully applied our quantitative 3D microscopy method to study the distribution of AAV2 particles in animal tissues. We and other groups have observed the limited spreading of AAV2 transduction around the needle track as indicated by the expression pattern of various reporter genes (**Figure 5a**).[34–36] However, there is no direct evidence on AAV2 trafficking that provides the molecular rationale for such transgene expression profiles *in vivo*. To address this question, we used the quantitative microscopy method to directly quantitate the distribution of AAV2 particles in mouse muscle over time. Our results for the first time showed that the AAV2 particles were localized at the injection site during the first 30 minutes and then uniformly spread through tissues up to three muscle fibers away from the injection site over 4 hours (**Figure 5b**). This result is significant in that it allows one to correlate viral spread with expression and should provide insight into vector tropism when studying capsid variants specific for muscle or various tissues such as brain and eye.[34,35,37–39] Another important question is how the viruses traffic to the cells distal from the injection site.[34,35,37–40] Transcytosis has been proposed as a mechanism for the spreading of various viruses, including HIV, poliovirus, and AAV, and most of these studies involved epithelial cell barriers using *in vitro* transwell cell culture.[40–42] However, little information is available regarding the mechanism of trafficking for AAV particles *in vivo*. Our studies using this quantitative 3D microscopy method show that almost all viral particles localized to the boundary of the muscle fibers (sarcoplasm) but not inside the fibers when trafficking to the distant fibers (**Figure 5b**). This observation strongly suggests that most AAV2 particles traffic through the endomysium between muscle fibers instead of traversing through myofibers. These virions

between muscle fibers, we believe, are infectious as indicated by the transgene expression in these muscle cells (**Figure 5a**). It is also noteworthy that the trafficking kinetics showing virions in muscle nuclei at 30 minutes to 4hours (**Figure 5b**) combined with the absence of AAV2 in nuclei at 6 days p.i. (**Figure 5c**) suggests that nuclear AAV2 vectors release their genomes quite rapidly. Previous reports demonstrated that the expression of AAV2 transgenes in muscle did not reach the peak until around 5 weeks p.i.[34,43] These studies in combination may support that, after uncoating, AAV2 transduction may be impacted by other cellular factors such as the rate-limiting step of second strand synthesis.[44–46] Additionally, at 6 days after injection, AAV2 particles were also detected inside of the muscle fibers/cells (**Figure 5c**). This observation supports a hypothesis that, unlike in cultured cells, viral particles *in vivo* can persist in myofibers potentially providing a temporal reservoir of virus. And these virions may traffic to the nucleus and contribute to viral transduction at later times (over 2 weeks), which also could be an explanation to the observed AAV transduction profile in muscle.[34,43]

This quantitative 3D distribution microscopy approach presented here was originally designed to quantitatively examine how pharmacological reagents and viral genetic variants impact the trafficking kinetics and biodistribution of viral vectors. With this approach, we have generated a panel of very interesting and biologically meaningful results consistent with previous reports as well as several novel observations that have not been previously documented. These findings both support the current working knowledge of AAV biology and provide a better mechanistic insight into the behavior of this viral vector *in vitro* and *in vivo*. It will be of particular interest to quantitatively compare the trafficking behavior of various AAV serotypes and chimeric vectors, as well as mutant capsids defective/enhanced in viral trafficking. Data from such studies should provide guidance for the rational design of optimal gene therapy vectors. Therefore, such an ability to quantitate the distribution and trafficking kinetics of nanoparticles (**Figure 6c**) should facilitate a quantitative evaluation of the effects of pharmacological reagents and vector variants on the delivery performance of these particles in cultured cells as well as animal tissues. Finally, in combination with pharmacological tools and live cell imaging, this 3D quantitative distribution microscopy approach will provide a comprehensive and powerful method to understand the physiological life cycle of gene-delivery vectors as well as the intracellular behavior of other nanoparticles *in vitro* and *in vivo*.

MATERIALS AND METHODS

Production and purification of viruses. Virus was produced in HEK-293 cells as previously described.[47] Briefly, using polyethylenimine (linear molecular weight, ~25,000), cells were triple transfected with pXR2, the pXX680 helper plasmid, and pTR-CMV-GFP containing the GFP reporter transgene flanked by inverted terminal repeats. At 60 hours posttransfection, cells were harvested and nuclei were isolated as previously described.[47] The nuclear pellet from 10 plates was resuspended in 10 ml phosphate-buffered saline (PBS) with 0.5% deoxycholate (DOC) and then sonicated for 1 minute. This suspension was incubated at 37 °C for 45 minutes in the presence of 100 µg/ml DNase. Virus suspension was subjected to one round of cesium chloride (CsCl) step gradient density (1.3 g/cm^3 and 1.5 g/cm^3) fractionation. The viral fraction that resided in the interface between the two gradients was collected and subjected to another round of fractionation using CsCl continuous gradient density. Fractions that contained peak virus titers as determined by both slot dot blots and SDS-PAGE electrophoresis were dialyzed against 1× PBS supplemented with 5% sorbitol. Viral titers were determined by both dot blot[47] and qPCR. The infectivity of AAV is determined to about 1 transduction unit per 100 particles.

Cy5 labeling of viral particles. AAV2 was covalently labeled with fluorophores as described.[48] AAV2 labeling followed essentially the same protocol with slight modification. Briefly, purified AAV2 was incubated for 1 hour at 4 °C in PBS with a tenfold molar excess of Cy5 mono *N*-Hydroxysuccinimide (NHS) esters (GE Healthcare, Piscataway, NJ) over the capsid protein units. Labeled viruses were separated from the free dyes by dialysis against PBS containing 5% sorbitol and stored at −80 °C as small aliquots. The degree of labeling (DOL) was determined by spectophotometry using DOL = A_{max} / ([virus] × E_{dye}), with A_{max} = absorbance of dye at absorbance maximum, [virus] = virus concentration, and E_{dye} = extinction coefficient of the dye at its absorbance maximum. Please refer to the manufacturer's instructions for further details. Labeled viral titers were determined by both dot blot[47] and qPCR.

Vector administration and animal studies. Housing and handling of BALB/c mice used in the current study were carried out in compliance with the National Institutes of Health guidelines and approved by the IACUC at the University of North Carolina–Chapel Hill. Recombinant AAV2 vectors packaging GFP transgenes were administered through the intramuscular (2×10^9 vg into the hind limb) in a volume of 20 µl PBS. At 0.5, 2, 4 hours and 6 days after intramuscular injection, animals received an overdose of pentobarbital (100 mg/kg intraperitoneally) and were perfused transcardially with ice-cold 100 mmol/l sodium PBS (pH 7.4), followed by 4% paraformaldehyde in PBS (pH 7.4). After muscle was postfixed for 24 hours at 4 °C in paraformaldehyde/PBS,[49] 15 µm cross-sections were cut using a cryosection microtome. Then the slides were directly sealed with mounting medium (Prolong Antifade Gold with DAPI; Molecular Probes, Eugene, OR).

Immunofluorescence. Similar to what we have previously described,[15] HeLa cells (3×10^4 per well) were plated on 12-mm glass coverslips at 24 hours before infection. Next day, after incubation in Dulbecco's Modified Eagle Medium containing 20 mmol/l 4-(2-hydroxyethyl)-1-piperazineethanesulfonic acid at 4 °C for 5 minutes, cells were incubated with Cy5-labeled virions (5,000 or 25,000 vg/cell) at 4 °C for another 40 minutes. Cells were washed three times with PBS to remove unbound viruses and transferred to 37 °C incubator (regarded as 0 hour p.i.). At the indicated time points, cells were washed with PBS and then fixed with 4% paraformaldehyde for 15 minutes at room temperature (RT). The cells were then permeabilized with 0.2% Triton X-100 in PBS for 5 minutes at room temperature. Following four washes with PBS, the permeabilized cells were blocked with immunofluorescence buffer (5% normal goat serum in PBS containing 0.05% Tween-20) for 1 hour at room temperature. The cells were incubated with primary antibody to detect Lamp1 (monoclonal from Santa Cruz Biotechnology, Santa Cruz, CA) diluted in 50% immunofluorescence buffer for overnight at 4 °C. The cells were then incubated in secondary antibody, diluted 1:2,000 in 50% immunofluorescence buffer (anti-mouse Alexa-Fluor 488 (Molecular Probes)), for 1 hour at room temperature. After six washes with PBS, coverslips were mounted cell side down on glass slides with mounting medium (Prolong Antifade Gold with DAPI; Molecular Probes).

3D confocal fluorescence microscopy and 3D blind deconvolution. The labeled HeLa cells were examined by use of a Zeiss LSM710 laser scanning confocal microscope equipped with a Zeiss Plan-Apochromat 63×/NA 1.40 oil objective. The confocal pinhole aperture was set to the diameter

of the first Airy disk. Stacks of 20–30 focal planes were captured at 0.31 µm *z*-intervals through the depth of the cell. 3D images of the cells were reconstructed by using the image stacks. The Nyquist theorem, which utilizes the limitation of the microscope optics (full width at half maximum) to dictate adequate sampling, was used to determine that pixel dimensions of 0.13 × 0.13 × 0.31 µm (X, Y, Z) were required to properly sample the data.

Deconvolution was performed by AutoDeblur software (Media Cybernetics, Bethesda, MD), using iterative and constrained algorithms. The procedure started with a theoretical PSF derived from the actual setting of Zeiss710 confocal microscope. To generate the theoretical PSF, AutoDeblur took the following factors into consideration: NA of the microscope objective, refractive index of the medium, excitation wavelength, emission wavelength, confocal pinhole radius, pixel size, *z*-axis interval, microscope type (*i.e.*, wide field, confocal), and number of excitation photons. A new adjusted adaptive PSF derived from the previous deconvolution round was used to generate next adaptive PSF that fits the real imaging data better than the previous one (termed as one iteration or deconvolution round[20]). The number of iterations may serve as a regularization factor. In general, the remaining restoration error decreases with an increasing number of iterations. At the same time, the error due to noise amplification increases. The procedure should be stopped at an iteration number in which the sum of both errors is minimal.[50] To determine the optimal number of iteration, intracellular Cy5-AAV2 particles were deconvolved up to 50 rounds and the resulting images were saved every five rounds. The resulting images from 10 deconvolution rounds (number of iteration) displayed the highest signal-to-noise ratio, best spatial resolution, and most closely resemble the fluorescence signal from a point light source (**Supplementary Figure S1b**). This iteration number (10 rounds) was then used to deconvolve all the confocal images in this paper.

Computer-assisted 3D visualization and analysis. All deconvolved image stacks was processed using IMARIS software package (Bitplane AG, Zurich, Switzerland) for visualization and quantification purpose. Briefly, a deconvolved image stack was reconstructed using a volume rendering module and smoothened by a 3D-median filter. Subsequently, an isosurface rendering module was applied through thresholding by the fluorescence intensity that is slightly higher than background. For Cy5-AAV2, the isosurface rendering was thresholded at the fluorescence intensity of 1,000 a.u. (the upper boundary of background). ForAF488-Lamp1, the fluorescence intensity of 530 a.u. was used. For DAPI, isosurface rendering was thresholded at the fluorescence intensity of 2,500 a.u. The parameters (volume, MFI, TFI) for these isosurface-coated Cy5-AAV2 objects were extracted from the IMARIS program and analyzed as described in Results section. The localization of Cy5-AAV2 in nucleus or lysosomes was analyzed as described in Results section. Aberrations caused by refractive index mismatch results in a suboptimal *z* resolution. Full width at half maximum changes of the PSFs of the two channels (DAPI and Cy5) differed one voxel (0.13 × 0.13 × 0.31 µm^3) in XY- and Z-directions, while no significant changes were observed between AF488 and Cy5. The channel registration difference between DAPI and Cy5 was fixed by adjusting the DAPI channel using channel shift module in IMARIS to avoid potential false-positive localization results.

Atomic force microscopy. After imaging with confocal microscope, the coverslips were removed from glass slides and gently rinsed with PBS. The coverslips were quickly rinsed in ddH_2O, blotted dry, and then slightly dried under a stream of nitrogen. The images were captured in air with a Nanoscope IIIa (Digital Instruments, Santa Barbara, CA) microscope in tapping mode. Pointprobe tapping mode silicon probes (Molecular Imaging, Tempe, AZ) with spring constants of ~50 N/m and resonance frequencies ~170 kHz were used for all imaging. The images were collected at a speed of 4 Hz, a size of 4 µm × 4 µm, and a resolution of 512 × 512 pixels.

Electron microscopy. Purified and dialyzed virus particles in 1× PBS were pipetted onto a glow-discharged copper grid. The grid was washed twice with water and then stained with 2% uranyl acetate. Electron microscopy images were taken with a LEO EM 910 transmission electron microscope at various magnifications.

SUPPLEMENTARY MATERIAL

Figure S1. Theoretical point spread function of confocal images and optimization of 3D deconvolution.
Figure S2. Total fluorescence intensity is proportional to the amount of dyes and dye-labeled beads.
Figure S3. Evaluation of AAV2 morphology and infectivity after chemical conjugation with Cy5.
Figure S4. Visualization of Cy5-AAV2 particles within cells by fluorescence microscopy.
Figure S5. Mean fluorescence intensity of single Cy5-AAV2 on coverslips and in cellular environment.
Figure S6. Association of Cy5-AAV2 with the lysosomes.
Figure S7. The level of transgene GFPsc expression at two different viral dosages.
Video S1. Isosurface rendering of Cy5-AAV2 fluorescence signal.
Video S2. Isosurface rendering–assisted 3D localization of Cy5-AAV2 particles in cell nucleus at 6 hours postinfection.
Video S3. Isosurface rendering reveals the localization of Cy5-AAV2 particles in HeLa cells at 0 hour after binding.
Video S4. Isosurface rendering reveals the localization of Cy5-AAV2 particles in HeLa cells at 2 hours after binding.
Video S5. Isosurface rendering reveals the localization of Cy5-AAV2 particles in HeLa cells at 8 hours after binding.
Video S6. Isosurface rendering reveals the spreading of Cy5-AAV2 particles in mouse muscle tissue at 2 hours after intramuscular injection.
Video S7. Isosurface rendering reveals the spreading of Cy5-AAV2 particles in mouse muscle tissue at 4 hours after intramuscular injection.

ACKNOWLEDGMENTS

This research was funded from the National Institutes of Health Grants 1R01AI080726 and 5R01DK084033-01 (to C.L. and R.J.S.), 5U54AR056953 and 5R01AI072176 (to R.J.S.). We thank members of the UNC Gene Therapy Center for productive discussions, specifically Aravind Asokan, Matthew Hirsch, Sarah Nicolson, Steve Gray, Thomas Bridges Lentz, and Tal Kafri. We also thank members in the laboratory of Ken Jacoboson, especially Dr Jacobson and Dr Neumann for providing informative suggestions and discussions. We thank Lu Huang in Cystic Fibrosis Center for statistical data analysis. We greatly appreciate Swati Yadav for calculating virus titers by qPCR. And we thank the members in the Microscopy Services Laboratory, especially Dr Bagnell and Steven Ray, and the Chapel Hill Analytical and Nanofabrication Laboratory (CHANL) for providing resources. We also acknowledge Robert Sons for helping edit the manuscript.

REFERENCES

1. Rissanen, TT and Ylä-Herttuala, S (2007). Current status of cardiovascular gene therapy. *Mol Ther* **15**: 1233–1247.
2. Warrington, KH Jr and Herzog, RW (2006). Treatment of human disease by adeno-associated viral gene transfer. *Hum Genet* **119**: 571–603.
3. Breunig, M, Bauer, S and Goepferich, A (2008). Polymers and nanoparticles: intelligent tools for intracellular targeting? *Eur J Pharm Biopharm* **68**: 112–128.
4. Brandenburg, B and Zhuang, X (2007). Virus trafficking - learning from single-virus tracking. *Nat Rev Microbiol* **5**: 197–208.
5. Bartlett, JS, Wilcher, R and Samulski, RJ (2000). Infectious entry pathway of adeno-associated virus and adeno-associated virus vectors. *J Virol* **74**: 2777–2785.
6. Asokan, A, Conway, JC, Phillips, JL, Li, C, Hegge, J, Sinnott, R *et al.* (2010). Reengineering a receptor footprint of adeno-associated virus enables selective and systemic gene transfer to muscle. *Nat Biotechnol* **28**: 79–82.
7. Maheshri, N, Koerber, JT, Kaspar, BK and Schaffer, DV (2006). Directed evolution of adeno-associated virus yields enhanced gene delivery vectors. *Nat Biotechnol* **24**: 198–204.
8. Yang, L, Jiang, J, Drouin, LM, Agbandje-McKenna, M, Chen, C, Qiao, C *et al.* (2009). A myocardium tropic adeno-associated virus (AAV) evolved by DNA shuffling and *in vivo* selection. *Proc Natl Acad Sci USA* **106**: 3946–3951.

9. Duan, D, Yue, Y, Yan, Z, Yang, J and Engelhardt, JF (2000). Endosomal processing limits gene transfer to polarized airway epithelia by adeno-associated virus. *J Clin Invest* **105**: 1573–1587.
10. Ding, W, Zhang, LN, Yeaman, C and Engelhardt, JF (2006). rAAV2 traffics through both the late and the recycling endosomes in a dose-dependent fashion. *Mol Ther* **13**: 671–682.
11. Schelhaas, M, Ewers, H, Rajamäki, ML, Day, PM, Schiller, JT and Helenius, A (2008). Human papillomavirus type 16 entry: retrograde cell surface transport along actin-rich protrusions. *PLoS Pathog* **4**: e1000148.
12. Akita, H, Ito, R, Khalil, IA, Futaki, S and Harashima, H (2004). Quantitative three-dimensional analysis of the intracellular trafficking of plasmid DNA transfected by a nonviral gene delivery system using confocal laser scanning microscopy. *Mol Ther* **9**: 443–451.
13. Ho, YP, Chen, HH, Leong, KW and Wang, TH (2006). Evaluating the intracellular stability and unpacking of DNA nanocomplexes by quantum dots-FRET. *J Control Release* **116**: 83–89.
14. Seisenberger, G, Ried, MU, Endress, T, Büning, H, Hallek, M and Bräuchle, C (2001). Real-time single-molecule imaging of the infection pathway of an adeno-associated virus. *Science* **294**: 1929–1932.
15. Johnson, JS and Samulski, RJ (2009). Enhancement of adeno-associated virus infection by mobilizing capsids into and out of the nucleolus. *J Virol* **83**: 2632–2644.
16. Zeltner, N, Kohlbrenner, E, Clément, N, Weber, T and Linden, RM (2010). Near-perfect infectivity of wild-type AAV as benchmark for infectivity of recombinant AAV vectors. *Gene Ther* **17**: 872–879.
17. Sedarat, F, Lin, E, Moore, ED and Tibbits, GF (2004). Deconvolution of confocal images of dihydropyridine and ryanodine receptors in developing cardiomyocytes. *J Appl Physiol* **97**: 1098–1103.
18. Feng, D, Marshburn, D, Jen, D, Weinberg, RJ, Taylor, RM 2nd and Burette, A (2007). Stepping into the third dimension. *J Neurosci* **27**: 12757–12760.
19. Chen, HH, Ho, YP, Jiang, X, Mao, HQ, Wang, TH and Leong, KW (2008). Quantitative comparison of intracellular unpacking kinetics of polyplexes by a model constructed from quantum dot-FRET. *Mol Ther* **16**: 324–332.
20. Pawley, JB (2006). Handbook of Biological Confocal Microscopy. Springer: New York.
21. Haffar, O and Bukrinsky, M (2005). Nuclear translocation as a novel target for anti-HIV drugs. *Expert Rev Anti Infect Ther* **3**: 41–50.
22. Suzuki, Y and Craigie, R (2007). The road to chromatin - nuclear entry of retroviruses. *Nat Rev Microbiol* **5**: 187–196.
23. Greber, UF and Puntener, D (2009). DNA-tumor virus entry–from plasma membrane to the nucleus. *Semin Cell Dev Biol* **20**: 631–642.
24. Sonntag, F, Bleker, S, Leuchs, B, Fischer, R and Kleinschmidt, JA (2006). Adeno-associated virus type 2 capsids with externalized VP1/VP2 trafficking domains are generated prior to passage through the cytoplasm and are maintained until uncoating occurs in the nucleus. *J Virol* **80**: 11040–11054.
25. Zhong, L, Li, B, Jayandharan, G, Mah, CS, Govindasamy, L, Agbandje-McKenna, M *et al.* (2008). Tyrosine-phosphorylation of AAV2 vectors and its consequences on viral intracellular trafficking and transgene expression. *Virology* **381**: 194–202.
26. Hofherr, SE, Adams, KE, Chen, CY, May, S, Weaver, EA and Barry, MA (2011). Real-time dynamic imaging of virus distribution in vivo. *PLoS ONE* **6**: e17076.
27. Zenklusen, D, Larson, DR and Singer, RH (2008). Single-RNA counting reveals alternative modes of gene expression in yeast. *Nat Struct Mol Biol* **15**: 1263–1271.
28. Summerford, C and Samulski, RJ (1998). Membrane-associated heparan sulfate proteoglycan is a receptor for adeno-associated virus type 2 virions. *J Virol* **72**: 1438–1445.
29. Whittaker, GR, Kann, M and Helenius, A (2000). Viral entry into the nucleus. *Annu Rev Cell Dev Biol* **16**: 627–651.
30. Hansen, J, Qing, K, Kwon, HJ, Mah, C and Srivastava, A (2000). Impaired intracellular trafficking of adeno-associated virus type 2 vectors limits efficient transduction of murine fibroblasts. *J Virol* **74**: 992–996.
31. Mudhakir, D and Harashima, H (2009). Learning from the viral journey: how to enter cells and how to overcome intracellular barriers to reach the nucleus. *AAPS J* **11**: 65–77.
32. Shen, S, Bryant, KD, Brown, SM, Randell, SH and Asokan, A (2011). Terminal N-linked galactose is the primary receptor for adeno-associated virus 9. *J Biol Chem* **286**: 13532–13540.
33. Heim, R, Cubitt, AB and Tsien, RY (1995). Improved green fluorescence. *Nature* **373**: 663–664.
34. Fisher, KJ, Jooss, K, Alston, J, Yang, Y, Haecker, SE, High, K *et al.* (1997). Recombinant adeno-associated virus for muscle directed gene therapy. *Nat Med* **3**: 306–312.
35. Kessler, PD, Podsakoff, GM, Chen, X, McQuiston, SA, Colosi, PC, Matelis, LA *et al.* (1996). Gene delivery to skeletal muscle results in sustained expression and systemic delivery of a therapeutic protein. *Proc Natl Acad Sci USA* **93**: 14082–14087.
36. Pruchnic, R, Cao, B, Peterson, ZQ, Xiao, X, Li, J, Samulski, RJ *et al.* (2000). The use of adeno-associated virus to circumvent the maturation-dependent viral transduction of muscle fibers. *Hum Gene Ther* **11**: 521–536.
37. Gregorevic, P, Blankinship, MJ, Allen, JM, Crawford, RW, Meuse, L, Miller, DG *et al.* (2004). Systemic delivery of genes to striated muscles using adeno-associated viral vectors. *Nat Med* **10**: 828–834.
38. Sun, B, Zhang, H, Franco, LM, Young, SP, Schneider, A, Bird, A *et al.* (2005). Efficacy of an adeno-associated virus 8-pseudotyped vector in glycogen storage disease type II. *Mol Ther* **11**: 57–65.
39. Wang, Z, Zhu, T, Qiao, C, Zhou, L, Wang, B, Zhang, J *et al.* (2005). Adeno-associated virus serotype 8 efficiently delivers genes to muscle and heart. *Nat Biotechnol* **23**: 321–328.
40. Di Pasquale, G and Chiorini, JA (2006). AAV transcytosis through barrier epithelia and endothelium. *Mol Ther* **13**: 506–516.
41. Bhat, P and Anderson, DA (2007). Hepatitis B virus translocates across a trophoblastic barrier. *J Virol* **81**: 7200–7207.
42. Bomsel, M and Alfsen, A (2003). Entry of viruses through the epithelial barrier: pathogenic trickery. *Nat Rev Mol Cell Biol* **4**: 57–68.
43. Chao, H, Liu, Y, Rabinowitz, J, Li, C, Samulski, RJ and Walsh, CE (2000). Several log increase in therapeutic transgene delivery by distinct adeno-associated viral serotype vectors. *Mol Ther* **2**: 619–623.
44. McCarty, DM, Monahan, PE and Samulski, RJ (2001). Self-complementary recombinant adeno-associated virus (scAAV) vectors promote efficient transduction independently of DNA synthesis. *Gene Ther* **8**: 1248–1254.
45. Ferrari, FK, Samulski, T, Shenk, T and Samulski, RJ (1996). Second-strand synthesis is a rate-limiting step for efficient transduction by recombinant adeno-associated virus vectors. *J Virol* **70**: 3227–3234.
46. Fisher, KJ, Gao, GP, Weitzman, MD, DeMatteo, R, Burda, JF and Wilson, JM (1996). Transduction with recombinant adeno-associated virus for gene therapy is limited by leading-strand synthesis. *J Virol* **70**: 520–532.
47. Grieger, JC, Choi, VW and Samulski, RJ (2006). Production and characterization of adeno-associated viral vectors. *Nat Protoc* **1**: 1412–1428.
48. Bartlett, JS, Samulski, RJ and McCown, TJ (1998). Selective and rapid uptake of adeno-associated virus type 2 in brain. *Hum Gene Ther* **9**: 1181–1186.
49. Xiao, PJ, Hu, L, Li, J, Lin, W, Chen, X and Xu, P (2007). NSSR1 is regulated in testes development and cryptorchidism and promotes the exon 5-included splicing of CREB transcripts. *Mol Reprod Dev* **74**: 1363–1372.
50. Vandervoort, HTM and Strasters KC (1995). Restoration of confocal images for quantitative image-analysis. *Journal of Microscopy-Oxford* **178**: 165–181.